Materials Characterization 156 (2019) 109849

Contents lists available at ScienceDirect

Materials Characterization

journal homepage: www.elsevier.com/locate/matchar

Experimental and numerical analyses of microstructure evolution of Cu-Cr-Zr alloys during severe plastic deformation

E.N. Borodin[a,*], A. Morozova[b], V. Bratov[c,d], A. Belyakov[b], A.P. Jivkov[a]

[a] Mechanics and Physics of Solids Research Group, School of MACE, The University of Manchester, Manchester M13 9PL, UK
[b] Belgorod State University, Pobedy 85, Belgorod 308015, Russia
[c] Institute of Problems of Mechanical Engineering RAS, 199178 V.O., Bolshoj pr., 61, St. Petersburg, Russia
[d] Saint-Petersburg State University, 199034 Universitetskaya nab., 7-9, Saint-Petersburg, Russia

ARTICLE INFO

Keywords:
Severe plastic deformation
Microstructural investigations
Continuous dynamic recrystallization
Triple junctions
Dislocations density
Numerical simulation
Grain boundary engineering

ABSTRACT

The focus of researchers studying severe plastic deformation on the final grain size of material is often preventing them from observing a much wider spectrum of alterations to material defect structure. It can be asserted that the decrease in material grain size is, in fact, only the consequence of many different processes accompanying plastic deformation in metals. We have performed a constitutive experimental, FEM and discrete complex based studies for two copper alloys subjected to ECAP and MDF deformation processes. This combination of methods allows for recognising complementary microstructural effects, such as micro- and macro-localization phenomena, coupled dislocation cells and grains evolution, inhomogeneities of triple junction network and ultrafine grain emergence. In many cases, the obtained deformational inhomogeneities play a substantial role both for deformation at macro- and microscale levels. Heterogeneity of grain boundary junction network could be critical for design of nanostructured copper-based alloys suitable for electrical applications.

1. Introduction

Methods of material processing using severe plastic deformation (SPD) are known for several decades and are attracting significant interest among researchers and industry [1–11]. SPD processing offers a possibility to create metallic materials possessing unique mechanical properties. In many cases tailored chemical and/or electrical properties can also be achieved. Presently, SPD techniques are still in the stage of active development [1,2,6,11]. Traditional and relatively simple methods, such as multidirectional forging (MDF) [4,7,9] or equal-channel angular pressing (ECAP) [4,7,10] provide a very wide range of possibilities for modification of properties in the bulk of a metallic material. Relatively new and perspective SPD methods include twist extrusion [1,4,7,11,12] and approaches using high-rate deformation [13,14]. Some of the modern methods comprise combinations and modifications of more traditional approaches, e.g. ECAP-conform process [4,15] and incremental ECAP [16], which have wide prospects for technological application. At this stage, the simpler methods are the most convenient for theoretical studies and numerical simulations of structural transformations accompanying SPD in metals. With respect to these, the most challenging issues are related to the prospects of industrial application of the processed materials [4,7,17]. The first industrial headway connected to the introduction of SPD-processed materials for medical applications [17] and for production of high-strength electric conductors [18] inspires new developments in the field.

The available models for the evolution of metal microstructure during deformation, however, are not sufficient for those industrial applications where robust prediction of a wide range of material properties *during* SPD is required. Existing approaches and models [19–24] usually involve and predict the evolution of a scalar quantity, the density of dislocations, and potentially the average grain size of the material at the end of SPD process. These models do not offer the possibility to involve and predict other microstructural characteristics that can be obtained experimentally and may have a substantial effect on the evolving macroscopic properties [3,25,26]. Among the most important and measurable microstructural characteristics are the fraction of high-angle grain boundaries (HAGBs), grain aspect ratio, properties of triple junctions including the presence of disclinations and stress concentrators in them. Considering the evolution of such parameters will enhance greatly the physical realism of models for continuous dynamic recrystallization (CDRX) process.

In principle, a set of microstructural characteristics for adequate characterization of fine-grain material microstructure has not been

* Corresponding author.
E-mail address: elbor7@gmail.com (E.N. Borodin).

https://doi.org/10.1016/j.matchar.2019.109849
Received 22 May 2019; Received in revised form 2 August 2019; Accepted 2 August 2019
Available online 07 August 2019

developed yet. Material grains and individual dislocations represent only the upper and the lower ends of material microstructure characteristics. Towards the lower end, dislocation character and a dislocation arrangement parameter have been used as additional microstructure descriptors [27]. Towards the upper end, the fractions of triple junctions with different numbers (0, 1, 2 or 3) of incident HAGBs have been proposed to serve as descriptors linking different microstructural and material properties [26]. An interesting and rather surprising feature was demonstrated in [26]: the fraction of triple junctions with one incident HAGB in copper alloys is significantly less than the fractions of triple junctions with 0, 2 or 3 HAGBs. This observation can be explained by considering that the new grain structure is not being formed homogeneously in the bulk of the material, but predominantly between the micro-bands of plastic flow localization. It is clear that such an explanation cannot be reflected by other commonly used averaged characteristics of the material microstructure.

The present work aims to further the understanding of microstructure-properties relations during SPD, firstly by extending the theoretical research initiated in [28] and then by complementing it with a novel discrete approach to analysis of such relations. The paper presents experimental and computational analyses of deformation of two copper alloys: Cu-0.1Cr-0.06Zr and Cu-0.3Cr-0.5Zr (wt%), each subjected to two different SPD processes: multidirectional forging (MDF) and equal-channel angular pressing (ECAP). Previously similar copper alloys were studied using different approaches [29–32], however these investigations were limited to the study of several basic material properties and were not including the detailed study of development of material microstructure in the process of deformation including the evolution of dislocation densities, grain sizes, cell sizes, HAGBs fraction and triple junctions (TJs). All of these parameters, which are necessary for detailed microstructure investigations, are obtained here from the original experimental data. The difference in the structure of Cu-0.1Cr-0.06Zr and Cu-0.3Cr-0.5Zr alloys leads to observed differences in evolution of their defect structure.

The experimental observations and measurements are used in the development of an improved theoretical description, implemented in a finite element framework. Simulations with the resulting model show that the microstructure evolution observed in our experiments for both alloys is predicted, to a large extent, by the proposed theoretical description. Specifically, results from 3D modelling of copper alloys subjected to ECAP and MDF processes: (i) demonstrate the opportunity to model different SPD processes with the same set of model parameters; and (ii) provide information about the magnitude of the macroscopic inhomogeneities of strain distribution within the bulk of the material after a single ECAP or MDF pass. This information is very important for correct estimations of plastic strain accumulated by the material in experiment. The complementary approach suggested in the paper is based on 3D discrete analyses of TJs network. The results are demonstrated to be in very close agreement with the experimental data and reveal the important role of micro-inhomogeneities observed in the experiments.

2. Experimental investigations of copper alloys processed by MDF and ECAP

2.1. Experimental setup

Two copper alloys with different alloying extent, Cu-0.1Cr-0.06Zr and Cu-0.3Cr-0.5Zr (wt%), were used in the present study. Following hot working, the low-alloyed Cu-0.1Cr-0.06Zr alloy was solution treated at 1093 K for 1 h followed by water quenching. Another cast alloy, Cu-0.3Cr-0.5Zr, was solution treated at 1193 K for 30 min followed by ageing at 723 K for 1 h with subsequent water quenching. Thus, the low-alloyed solution treated alloy with a grains size of 150 μm and the dispersion hardened alloy with a grain size of 700 μm and tiny chromium particles with a size of 10 nm were obtained in order to carry out a comprehensive analysis of the regularities of microstructure evolution in Cu-Cr-Zr alloys subjected to severe plastic deformation.

The copper samples were subjected to equal channel angular pressing (ECAP) and multidirectional forging (MDF) to clarify the effect of processing method on the microstructure evolution. Both ECAP and MDF were carried out at 673 K. The samples with starting dimensions of 14 mm × 14 mm × 80 mm were machined for ECAP, which was carried out with a pressing speed of 5 mm/s via route B_C (90° anticlockwise rotation of the sample after each pass). A true strain of 1 was imposed to the sample in each ECAP pass. Each ECAP sample was water quenched after desired ECAP pass number. The prismatic samples with initial dimensions of 25 mm × 20 mm × 16 mm were machined for MDF. MDF was carried out by means of isothermal compressions with a pass strain of 0.4 at a strain rate of $10^{-3}\,s^{-1}$ and a change of the compression direction through 90° from pass to pass. The MDF samples were water quenched and ground to prismatic shape after each pass.

The structural observations were performed on the sections parallel to the final pressing/forging direction using a Quanta 600 FEG scanning electron microscope equipped with an electron back scattering diffraction (EBSD) analyzer incorporating an orientation-imaging microscopy (OIM) and a Jeol JEM-2100 transmission electron microscope equipped with an INCA X-ray energy-dispersive spectrometer. The OIM images were subjected to clean-up procedures, setting a minimal confidence index of 0.1. An average grain size (D) was estimated using the linear intercept method on the OIM images as a distance between high-angle boundaries (HAB) with misorientation of $\theta \geq 15°$. The subgrain size (d) was estimated by the linear intercept method on the TEM micrographs counting all the clear visible boundaries/subboundaries. The dislocation densities were estimated using kernel average misorientations (θ_{KAM}) over a distance of 400 nm [33].

2.2. Deformation microstructures

Typical microstructures evolved in Cu-Cr-Zr alloys during severe plastic deformation are shown in Fig. 1. The deformation microstructures in the copper alloys subjected to ECAP and MDF have been considered in detail in previous studies [29,34]. The effects of chemical composition, dispersed particles and processing method on the main sequences of structural changes during severe plastic deformations can be briefly reviewed here as follows. Early deformation brings about the evolution of high dislocation density and the strain-induced subgrain/cell boundaries followed by the development of microshear bands crossing over the initial grains. Subsequent deformation is accompanied with an increase in the misorientations of strain-induced dislocation subboundaries. It is worth noting that the deformation subboundaries associated with microshear bands are characterized by faster kinetics of the misorientation evolution as compared to incidental subgrain/cell boundaries. An increase in the misorientations of deformation subboundaries above a critical HAGB angle (15°) allows considering them as strain-induced grain boundaries. Therefore, a number of strain-induced grain boundaries develop along with the microshear bands in the copper alloys at intermediate strains irrespective of chemical composition and processing method (Fig. 1). A progressive increase in the subboundary misorientations is testified by numerous incomplete grain boundaries, which are essentially the portions of strain-induced subboundaries with misorientations above a critical HAGB angle, in Fig. 1. The number of HAGBs increases as a result of gradual evolution of deformation subboundaries into strain-induced grain boundaries upon further deformation to sufficiently large total strains, leading to the development of ultrafine grained (UFG) microstructures. It should be noted that the dispersion strengthened alloy with relatively high alloying content exhibits faster kinetics of grain refinement than the initial solution treated low-alloyed one. Also, the sizes of grains and subgrains are smaller in the dispersion hardened Cu-0.3Cr-0.5Zr alloy than in the solution treated Cu-0.1Cr-0.06Zr one.

Fig. 2 shows the fine structures that developed in deformation

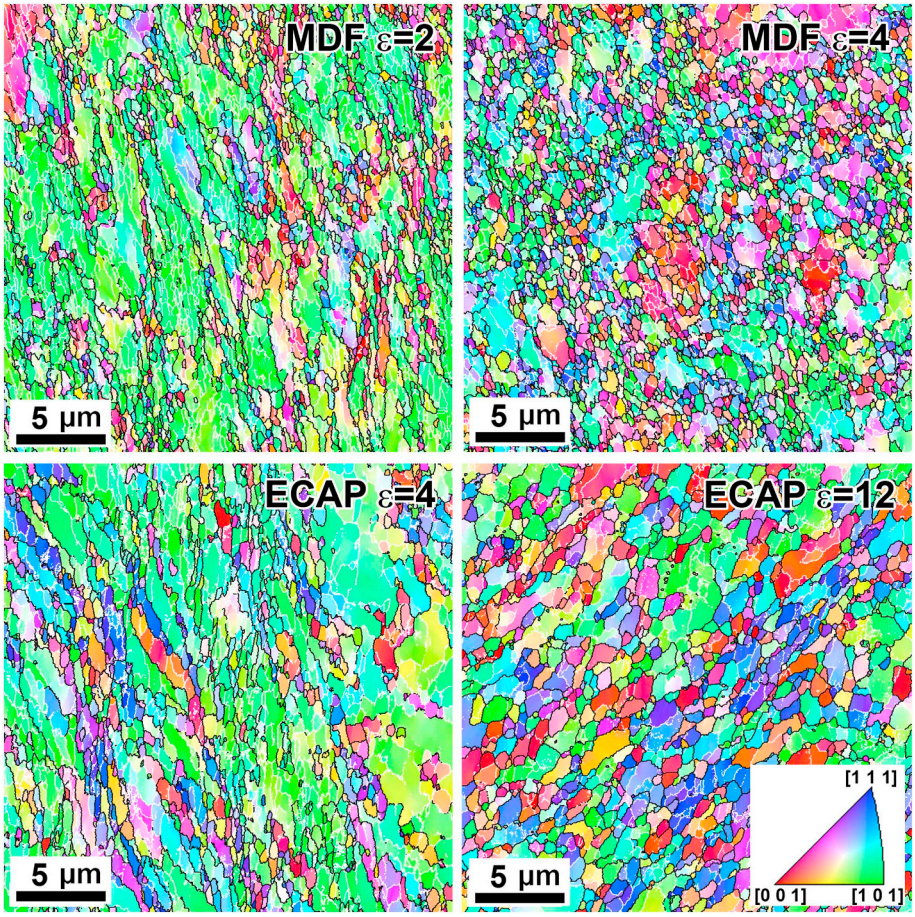

Fig. 1. Typical microstructures evolved in the Cu-0.3Cr-0.5Zr alloy during MDF to strain of ε = 2 (a) and ε = 4 (b), and those in the Cu-0.1Cr-0.06Zr subjected to ECAP to total strain of ε = 4 (c) and ε = 12 (d). Low- and high-angle boundaries are indicated by white and black lines, respectively.

microshear bands in more detail. It is clearly seen in Fig. 2a that the microshear band, which developed in the aged Cu-0.3Cr-0.5Zr alloy at a strain of 2, involves a frequent net of low-to-high angle (sub)boundaries. Hence, the microshear band consists of a grain-subgrain mixture and can be considered as a preferable nucleation site for UFG development. The ultrafine grains readily evolve in microshear bands during severe plastic deformation (Fig. 2b). In contrast to the dispersion hardened Cu-0.3Cr-0.5Zr alloy, the solution treated Cu-0.1Cr-0.06Zr alloy is characterized by lower dislocation density that results in smaller misorientation angles of dislocation subboundaries evolved at the same strain levels (cf. Fig. 2a and c). Moreover, the Cu-0.1Cr-0.06Zr alloy exhibits sluggish kinetics of the UFG development. The microshear band evolved at a total ECAP strain of 2 in this alloy is composed of mainly low-angle dislocation subboundaries (Fig. 2c). Nevertheless, an increase in the total strain results in the UFG development along the micro-shear bands in the low-alloyed solution treated Cu-0.1Cr-0.06Zr alloy as well (Fig. 2d).

3. Analysis methods

3.1. Theoretical considerations

Clearly, the correct description of the presented experimental results is not possible utilizing a simple model coupling the evolution of grain size to the plastic strain accumulated by the material. The proposed in [28] theoretical model for continuous dynamic recrystallization (CDRX) is an approach based on an assertion that the alternation of the material grain size is the consequence of essentially dynamic processes in the dislocation substructure on the microscopic level. The process of grain evolution is primarily determined by the rate of the ongoing dislocation processes and the features inherent to the formed triple and quadruple grain boundary junctions.

Dislocation kinetic and grain boundary evolution give a strain hardening of the material. The Taylor law and the Hall–Petch law [35] are the familiar relationships, which give an accurate prediction for the dynamic yield stress in the form

$$\sigma_D^0 = \sigma_y^0 + \alpha G b\sqrt{\rho_D} + K_{HP}/\sqrt{d}\,, \tag{1}$$

where σ_y^0 is static yield stress of the material without dislocations, which includes all internal stress concentrators except the dislocations or grain boundaries [28], $\alpha = 0.4$ is the Taylor constant [35], G is the shear modulus of the material, b is the Burgers vector, ρ_D is the dislocation density, K_{HP} is the Hall–Petch coefficient, and d is the (average) grain diameter. Total dislocation density is a sum of mobile (inside the grains) and immobile (along the grain boundaries) densities [28] $\rho_D = \rho_D^{mob} + \rho_D^{im}$. Modifying the equations proposed in [36] for dynamical deformation regimes, the evolutions of dislocation densities can be described with the following kinetic equations:

$$\frac{d\rho_D^{mob}}{d\varepsilon} = k_g\left(b\sigma_y^0 + \alpha G b^2\sqrt{\rho_D^{im} + \rho_D^{mob}}\right) - \frac{V_C\left(\rho_D^{mob} - \rho_D^0\right)\sqrt{\rho_D^{im}}}{\dot{\varepsilon}_{pl}}$$

$$- k_\alpha^m\left(2\rho_D^{mob} + \rho_D^{im}\right)\frac{d\rho_D^{im}}{d\varepsilon} = \frac{V_C\left(\rho_D^{mob} - \rho_D^0\right)\sqrt{\rho_D^{im}}}{\dot{\varepsilon}_{pl}} - k_\alpha^m\rho_D^{im} \tag{2}$$

where $k_g = \eta/\varepsilon_L b$ is the dislocation generation coefficient [36], k_α^m is the dislocation annihilation coefficient, which we assume to be the same for mobile and immobile dislocations, ρ_D^0 is a dislocation density threshold after which dislocation structures can exist, and V_C is the

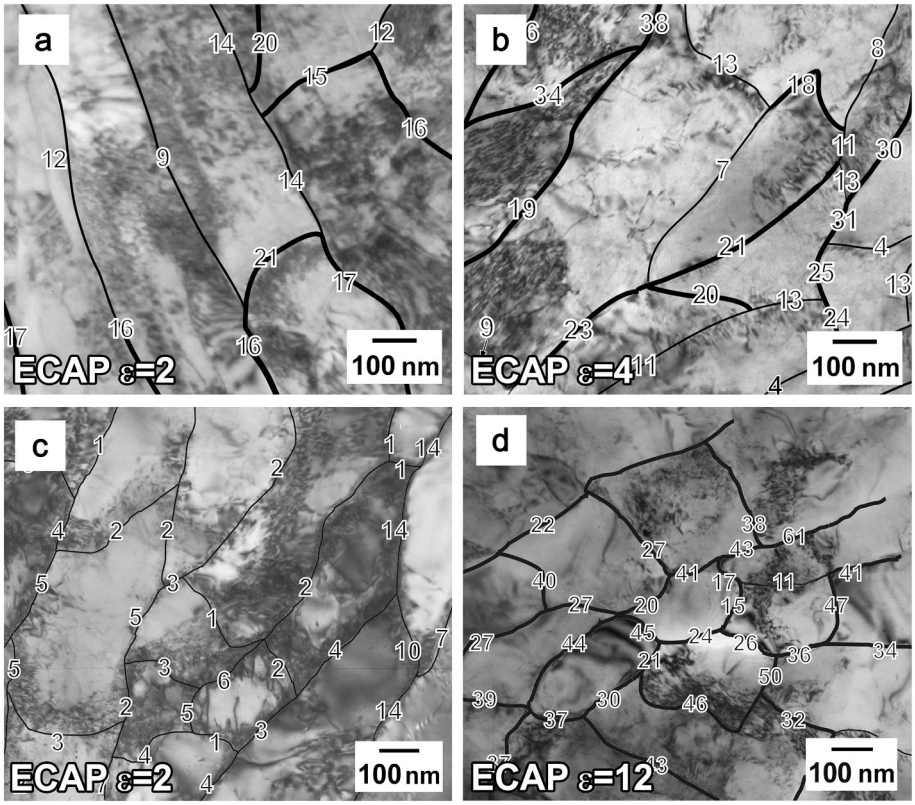

Fig. 2. Deformation substructures evolved in the Cu-0.3Cr-0.5Zr alloy subjected to ECAP to total strain of $\varepsilon = 2$ (a) and $\varepsilon = 4$ (b), and those in the Cu-0.1Cr-0.06Zr subjected to ECAP to total strain of $\varepsilon = 2$ (c) and $\varepsilon = 12$ (d). The numbers indicate the boundary misorientations in degrees.

velocity describing the transition between the two groups of dislocations [36]. The majority of these parameters, appearing in similar different logistic-type equations for dislocation densities [19,37], are well studied and different physical-based models are proposed for their estimation [38–43].

Correct prediction of the grain size evolution at CDRX is possibly the biggest challenge in the area of theoretical research of SPD processes. Following [28] we describe this evolution with two variables: the average dislocation cell diameter and HAGBs fraction. Dislocation cell diameter as a function of dislocation density can be written in the form [19,21,37,40,44]:

$$D = \beta \rho_D^{-1/2}. \tag{3}$$

Here β is a coefficient dependent on the shape of dislocation cells. There are several physical models for its analytical evaluation [40], which have shown that for an adequate description of dislocation cell network evolution it must have value at least 15–30.

To predict grain size evolution, d, in the same way as the cell size evolution (Eq. (3)), the parameter β cannot be treated as a constant, but must became a function of the deformation, reducing by a factor of 5 with the reduction of grain size from tens of micrometres to hundreds of nanometres [30]. In line with the presented experimental results, we refer to the cell sizes as the distances between low angle dislocation boundaries, and to the grain sizes as the distances between HAGBs boundaries. Then the most natural way to define the grain size is

$$d = \frac{D}{J}, \tag{4}$$

where J is a function from HAGBs fraction. For a homogeneous distribution of HAGBs through the material $J = p$ [28].

The central point of our further consideration of CDRX is that HAGBs cannot be formed as a result of uninterrupted evolution of dislocation boundaries. Apparently, the increase of misorientation angle across the grain boundary (i.e. transformation of LAGBs into HAGBs) requires a non-equilibrium state when a dislocation boundary is being "bombarded" by lattice dislocations accompanied with their active annihilation. Within the framework of this concept of non-equilibrium nature of transformation of LAGBs into HAGBs under the influence of the process of immobilization of dislocations at the boundary and the process of dislocation annihilation, we postulate that rate of non-equilibrium grain boundaries fraction change is proportional to the ratio of mobile to immobile dislocations V_C. Then, according to Eq. (2):

$$\rho_D^{V_C^{(-)}} = V_C(\rho_D^{mob} - \rho_D^0)\sqrt{\rho_D^{im}}. \tag{5}$$

In this case, the growth rate of nonequilibrium (potentially HAGBs) boundaries fraction can be presented as [28]:

$$\dot{p} = \chi \rho_D^{V_C^{(-)}} d/D. \tag{6}$$

Here χ is an empirical parameter with the value of about 10.

3.2. Finite element implementation

The plasticity model based on the above theoretical considerations was implemented as USERMAT FORTRAN subroutine for ANSYS commercial finite element software. The model and the implementation are similar to the ones described in [28]. The developed subroutine is executed during element result calculation and provides a possibility to update local dislocation densities as well as the other microstructure-related parameters in every point of the deformed sample. The parameters controlling microstructure evolution are updated at every time integration sub-step according to the local material deformed state. Since the process can be simulated as quasi-static, time integration is not performed. The problem is formulated as a number of consequent static sub-steps given by displacements gradually applied to the moving

Table 1
The main parameters used for simulations.

Model parameters	Immobilization rate	Annihilation coefficient	Coefficient of generation	Empirical parameter	Taylor constant	Empirical parameter
Values	$7.5 \cdot 10^{-8}$	1.9	$5.5 \cdot 10^{16}$	9.6	0.4	15
Material parameters	Shear modulus	Burgers vector	Temperature	Static yield stress	Initial dislocation density	Initial grain size
Values	46GPa	0.256 nm	673 K	130 MPa	10^{13} m^{-2}	100 mkm

part of the multidirectional forging die. Time is eliminated from state equations. Stresses and strains in the deformed specimen on each substep are calculated according to the elastic deformation model. Once a stress at some point of the bar reaches the value outside von Mises plastic flow surface, plastic flow is onset at this point. The strain that appeared at that point due to displacement applied at the top of the bar is split into elastic and plastic parts, returning the stress to the plastic flow surface. Alteration of the plastic part of strain tensor is affecting dislocation densities as well as the rest of the described material microstructure parameters. All necessary for simulation with model (1)–(5) material parameters are given in Table 1.

3.3. Discrete complex representation

In addition to the finite element representation of the materials as continua, we consider the 3-dimensional grain structure of copper alloys as a discrete complex [46], which for simplicity here is constructed by a Voronoi tessellation around a random set of points. Voro++ free software has been used for tessellations [47]. Two examples of discrete complexes with sizes 100 and 500 cells are shown in Fig. 3a, b. Another feature of Voro++ output is the possibility to set a certain volume distribution of grain sizes. Fig. 3c illustrates the normal-like grain size distribution of the complexes (a) and (b).

The distinct components of the combinatorial discrete complex are nodes (0-cells), edges (1-cells), faces (2-cells) and volumes (3-cells). For our physical consideration, volumes are associated with grains, faces with grain boundaries, edges with triple junctions and nodes with quadruple points, reflecting full polycrystalline structure of the materials. The analyses using the complex representation in this work will focus on the behaviour of triple junctions with deformation. Our calculations show that for complexes containing > 200–300 grains all relationships between its triple junctions become quite smooth and additional growth of the complex elements number is not required.

To analyze the discrete complex and to determine its topological characteristics a C/C++ code *VoroCAnalyser* (*VCA*) [48] has been written. This code gives a set of matrices, which characterise the complex fully. Among them are 4 sets of the elements' neighbours, an array with degree (number of neighbours) for each element and 3 incidence matrices: nodes-edges, edges-faces and faces-grains. All these matrices and arrays provide all information about relations inside the discrete complex. Actually, from the mathematical point of view, the discrete complex is a superposition of four graphs' structures, corresponding to the cells of each type. Interrelations between these graphs are given by the boundary operators represented by the set of incidence matrices. Any physical process defined on the elements of these graphs can be represented as a temporal change in the elements of the corresponding incidence matrices. This means that it can be expressed as the changes in the internal connectivity of the discrete complex. The connectivity matrices describing discrete complex representations of the alloys studied are used for all analyses presented in the next section.

4. Results and discussion

4.1. Finite element simulation results

The geometry corresponding to experimental conditions realized in the experiments presented in Section 2 is modelled. Essentially three-dimensional nature of deformation for multidirectional forging requires 3D numerical simulations to describe the process. Behaviour of material in ECAP experimental conditions can be successfully simulated utilizing 2D model (see ex. [28]). The main goal for the 2D numerical simulations of ECAP and the 3D numerical simulations of MDF was to study the degree of macroscopic inhomogeneity in distribution of stresses, strains and dislocation densities in the processed samples. Fig. 4 shows the distribution of accumulated plastic strain following the first pass of the ECAP (a) and the MDF (b) process.

The presented results show significant macroscopic inhomogeneity in distribution of plastic strain within the bulk of the material. For both samples presented, maximum plastic strains are achieved at the central part. For MDF maximum plastic strains are exceeding the average strain (0.4) more than twice and can reach values close to 1. For ECAP process, maximum strains are exceeding the average strain (1.0) only in a small region and not more than by 25%. According to the obtained results, for material processed by MDF, plastic strains at the corners of the sample can reach 2.5 or even more. In real experiments, these zones are usually removed between MDF passes and thereby can be not

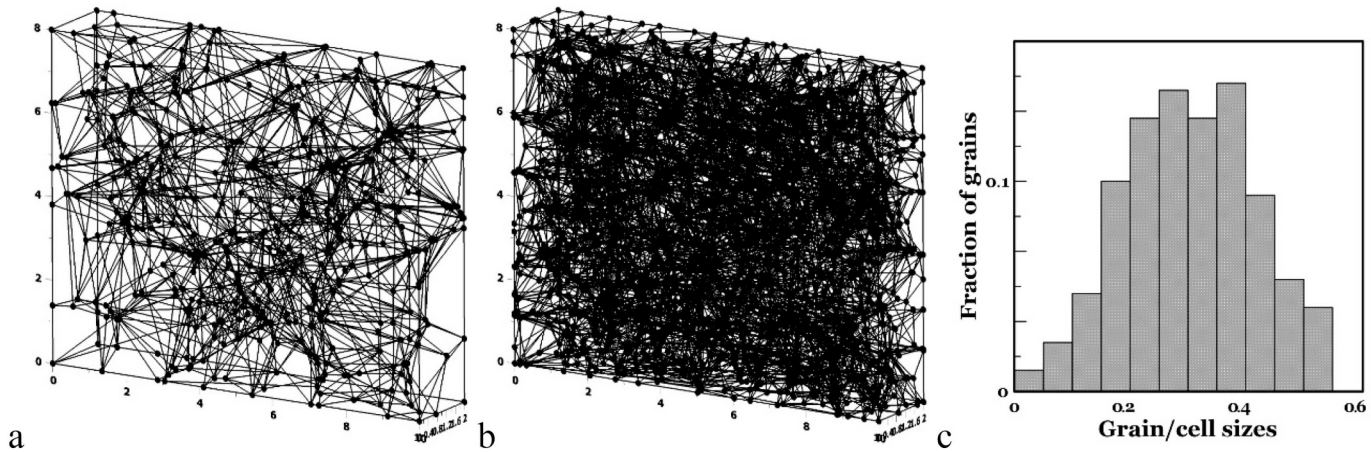

Fig. 3. Discrete complexes with 100 (a) and 500 (b) 3-cells (grains) obeying the normal grain size distribution (c).

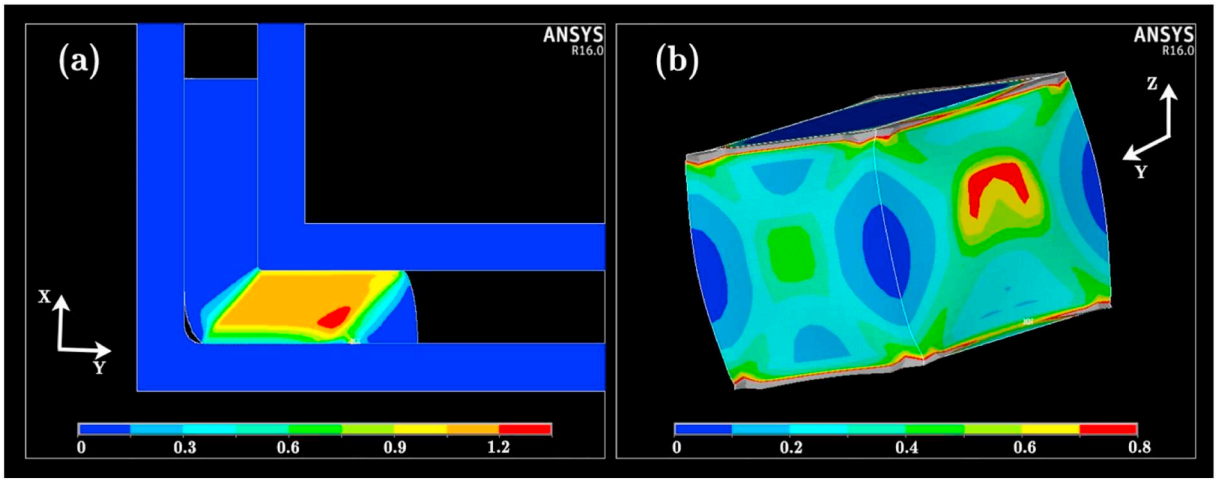

Fig. 4. Deformation (contour plot) of the sample after the single pass of ECAP (a, 2D model) and MDF (b, 3D model). For MDF sample, for clarity, the die is removed from presentation and only the sample is shown.

accounted for in numerical simulations.

Inhomogeneity of strain distribution is accompanied by the inhomogeneity of distribution of defect density, and according to Eq. (1) of the yield stress. The results for MDF and ECAP are shown in Figs. 5 and 6, respectively. Maximum dislocation density $\rho_D = \rho_D^{mob} + \rho_D^{im}$ attained within the material is around 10^{15} m^{-2} for both SPD processes. For MDF the obtained dislocation densities are slightly larger compared to ECAP of the same material.

Fig. 7(a) shows the computed by Eq. (2) dependencies of dislocation densities on accumulated strain. These are in a good agreement with the values measured experimentally. Points measured for MDF processed material for strains below 2 almost coincide with the values for the same material processes with ECAP. The large discrepancy between the measured dislocation density values for MDF and ECAP for strain equal to 4 requires further investigation of dislocation density behaviour for large values of deformation. Two-dimensional modelling gives two additional points marked with asterisks. The initial stage of material deformation in Fig. 7(a) is accompanied by intensive generation of mobile dislocations, reaching maximum density of mobile dislocations for strains ~1 and not changing significantly for plastic strain exceeding 2.

Additional dislocation drain, accounting for the intrusion of dislocations into grain boundaries and decrease of dislocation density due to transformation of cell walls into grain boundaries can be included

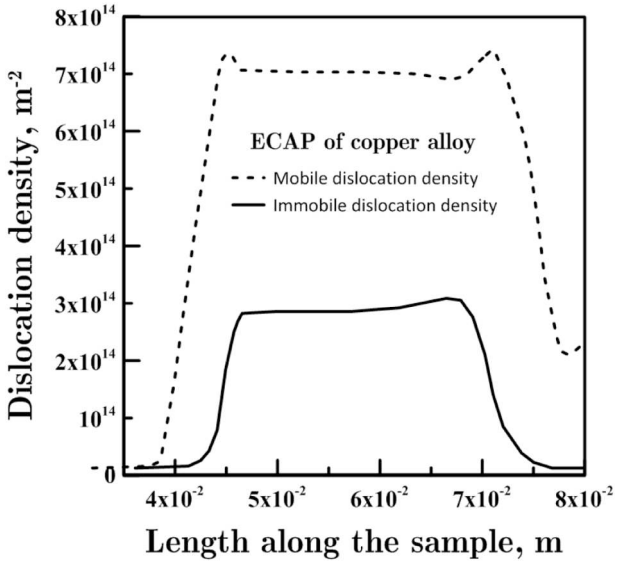

Fig. 6. Distribution of dislocation densities ρ_D^{mob}, ρ_D^{im} along the central axis of the sample for ECAP.

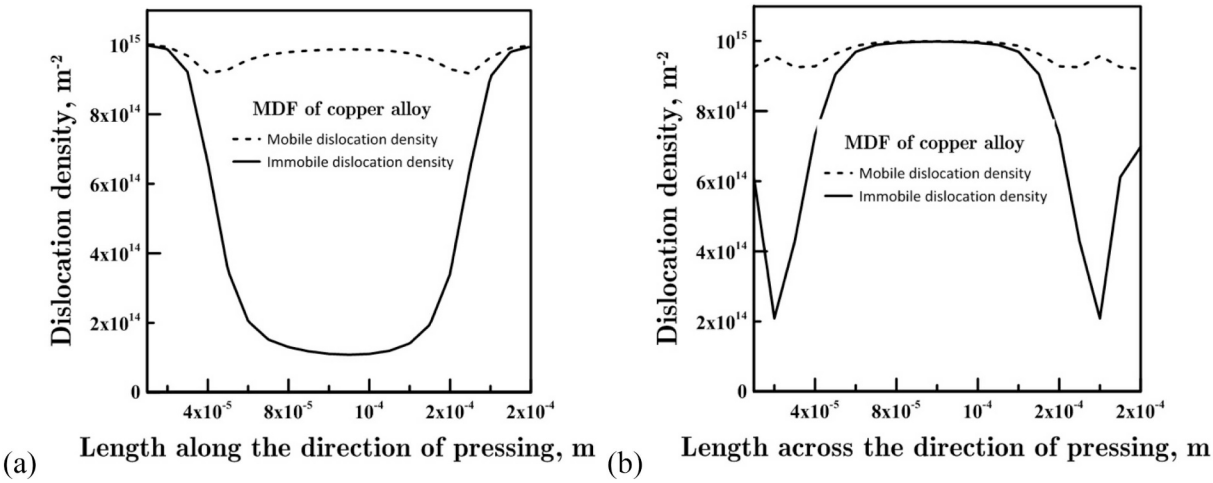

Fig. 5. Distribution of dislocation densities ρ_D^{mob}, ρ_D^{im} thorough the sample volume for MDF (cross-section in the central plane) along (a) and across (b) the direction of pressing that corresponds Z and Y direction in Fig. 4(b).

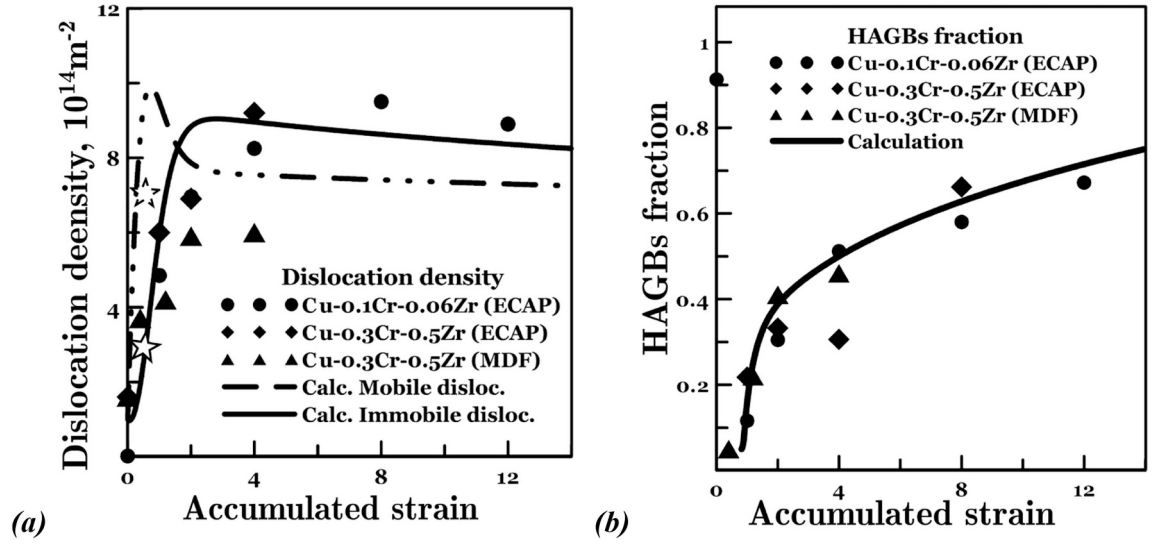

Fig. 7. (a) Density of mobile and immobile dislocations as a function of plastic strain accumulated by the material. Calculations using Eq. (3) (lines) are compared to experimental measurements (dots) of average dislocation density for the two copper alloys subjected to ECAP and MDF. Asterisks correspond to the results of 2D simulations of ECAP process. (b) Fraction of High-Angle Grain Boundaries (HAGBs) as a function of plastic strain accumulated by the material. Theoretical predictions (solid line) are compared to experimental measurements (dots) of HAGBs fraction for ECAP and MDF processed copper alloys.

into the first of the Eq. (2):

$$\rho_D^{(-)} = \rho_D V_D / d. \tag{7}$$

Here V_D is the average dislocation velocity [36]. This additional drain is responsible for the convergence of densities of mobile and immobile dislocations observed for large values of accumulated plastic strain. Furthermore, Eq. (7), similarly to the one presented in [22], leads to maximization of density of immobile dislocations for plastic strains ~2.

Fig. 7(b) presents a comparison of calculations using Eqs. (2)–(4) and (6) with the parameters listed in Table 1 with our experimental measurements. The large deviation between the first experimental point for initial material on the figure and the calculated curve is due to the initial state of coarse-grained material for which the fraction of HAGBs is usually very high. Already after the first pass of MDF this fraction is reduced in experiments by a factor of 10 due to formation of lower scale structure with low angle cell boundaries. The quasi-linear growth with two different slopes, before and after deformation equal 2, is accurately modelled by Eq. (6). Immobilization rate for lattice dislocations determined by V_C and the flow of cell dislocations onto the boundary determined by ρ_D^{mob} control this process. Experimental points for HAGBs fraction and its theoretical fitting with Eq. (7) are shown in Fig. 7(b). Both experimental data and theoretical curve change their slope dramatically around accumulated strain of 2. This function will be used as the main material characteristic in the next section for discrete simulation of the CDRX process.

Fig. 8 gives experimental points and theoretical curves calculated according to Eqs. (3) and (4) for the average size of dislocation cells and the average size of grains for SPD processed copper alloys. Least deformation is needed for evolution of dislocation cells: according to Fig. 8, average dislocation cells diameter is reduced several times already at strain ~1.

The experimental results presented in Fig. 7 show that MDF and ECAP processes do not yield significantly different grain size distributions, suggesting they can be approximated by a single theoretical curve. Unfortunately, the present experimental investigation is not providing information about behaviour of copper alloys subjected to MDF for strains exceeding 4. Behaviour of Cu-0.1Cr-0.06Zr alloy is substantially different from the behaviour of Cu-0.3Cr-0.5Zr alloy. For large values of accumulated plastic strain, grain and cell sizes observed at Cu-0.1Cr-0.06Zr alloy are almost twice the sizes observed for Cu-0.3Cr-0.6Zr. Obviously, the reason for that is the higher degree of inhomogeneity of Cu-0.3Cr-0.6Zr alloy, which can be reflected by consideration of the grain boundary triple junctions (TJs) evolution during the deformation process.

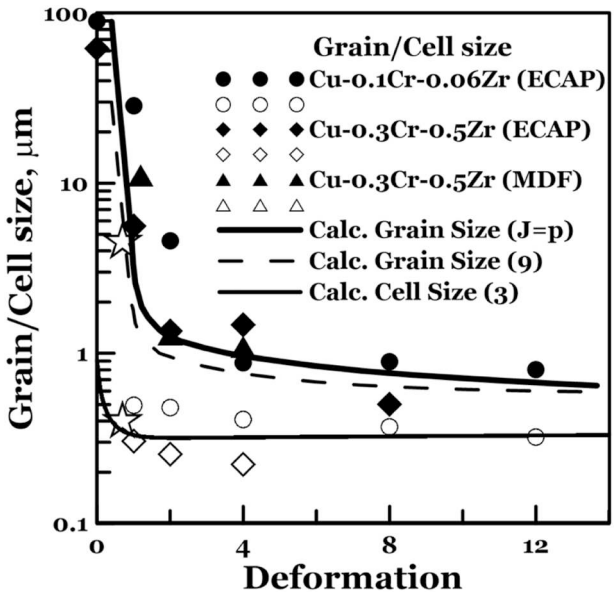

Fig. 8. Grain (dots) and cell (empty dots) size as functions of accumulated strain. Theoretical predictions using Eq. (13) (solid line) are compared to experimental measurements (dots) for ECAP and MDF processed copper alloys. Asterisks correspond to the results of 2D simulations of ECAP process.

Consider different types of TJs with 0, 1, 2 or 3 adjacent HAGBs, denoted as F_{J0}, …F_{J3} accordingly. For the homogeneous distribution of all types of grain boundary junctions a first approximation of the dependencies of TJs fractions from HAGBs fraction could be obtained by [45]:

$$F_{J0} = (1-p)^3;\ F_{J1} = 3p(1-p)^2;\ F_{J2} = 3p^2(1-p);\ F_{J3} = p^3 \tag{8}$$

It should be noted, that here our notations are inverse to the same ones in [49], where p means LAGBs fraction and correspondingly J_i are the fractions of TJs with i adjacent LAGBs. Obviously,

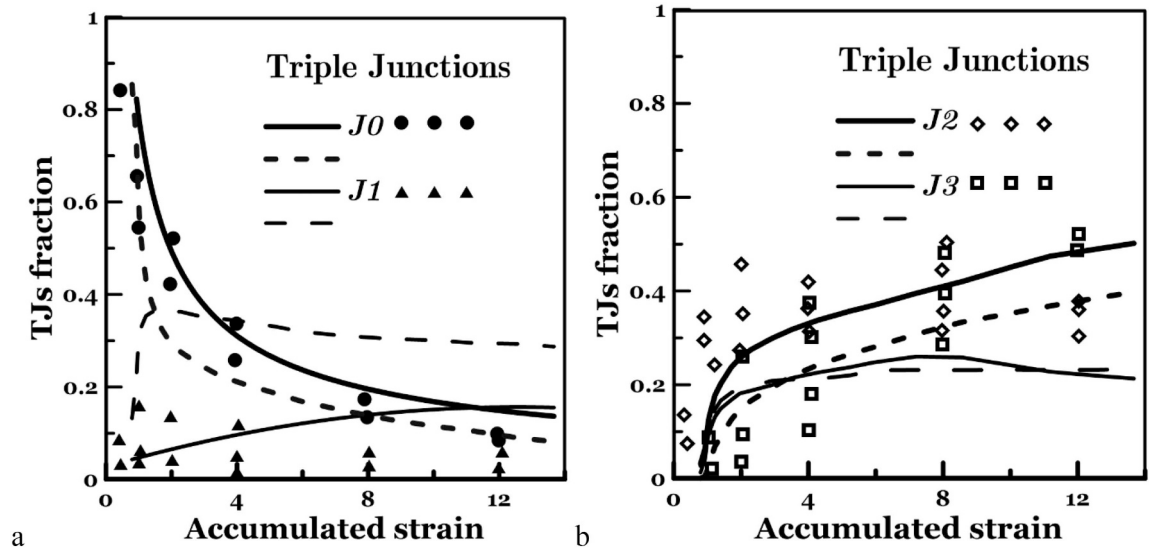

Fig. 9. The evolution of TJs structure during SPD process with purely random and "localized" methods for new HAGBs generation. Symbols represent experimental data points [26]. Dashed lines correspond to pure random generation of new HAGBs. Solid lines correspond to "localized" mode of new HAGBs generation, Eq. (12).

$p_{HAGBs} = 1 - p_{LAGBs}$, and $J_i^{HAGBs} = J_{3-i}^{LAGBs}$ that leads to the validity of the Eq. (8) for both cases because of its symmetry.

The real grain structure evolution is more complex as it was discussed earlier. It was shown that for studied copper alloys micro-localization within the grains is leading to F_{J0}, …F_{J3} distributions with F_{J1} being significantly less as comparing to the other components. In order to represent a slightly inhomogeneous microstructure the parameter J in Eq. (4) could be formulated in the form:

$$J = \frac{F_{J1} + 2F_{J2} + 3F_{J3}}{3} \tag{9}$$

Substitution of Eq. (8) into Eq. (9) recovers the case $J = p$. From the other hand at final stage, when $F_{J1} = F_{J2} = 0$; $F_{J3} = 1$, substitution of Eq. (9) into Eq. (4) gives true equality $d = D$. It needs to be clarified that Eq. (9) assumes that all types of TJs have essentially homogeneous distributions, while this is not required for the grain boundary types. So, without assuming that Eq. (8) holds, but following the experiments [26], we estimate the fractions of GBs as follows: $F_{J0} = 0.8 \cdot Exp[-0.25\varepsilon]$, $F_{J1} \sim 0.06$, $F_{J3} = 0.54 \cdot (1 + Exp[-0.56\varepsilon + 2.4])^{-1}$ and $F_{J2} = 1 - F_{J0} - F_{J1} - F_{J3}$, where we use the constraint $\Sigma_k F_{Jk} = 1$. The effect of the slight inhomogeneity introduced by these fractions is shown in Fig. 8 as a dotted line below the curve corresponding to $J = p$. Obviously, micro-inhomogeneities can influence significantly the microstructure-properties relations of the material, without changing noticeably its grain structure. The investigation of the grain size evolution based on a discrete complex analysis in the next sub-section removes the restrictions of any continuous approach and allows for simulating CDRX process directly as a stochastic one.

4.2. Discrete simulations of CDRX processes

For the calculations on the discrete complex, the accumulated strain is considered as a time-like variable instead of the physical time. This way the CDRX process is driven by prescribed fractions of HAGBs, i.e. during each calculation step a number of LAGBs are changed to HAGBs according to experimentally measured HAGBs fraction evolution shown in Fig. 7(b). There are different ways to decide which LAGBs are subject to this transition. The simplest one is the random conversation of LAGBs to HAGBs. It is actually an example of the random (the Erdős–Rényi) graph realization, where graph edges are introduced between neighbouring HAGBs. Hence, during a simulation step, when any two neighbouring faces in the discrete complex became HAGBs a new edge is introduced in the random graph and the degrees of both faces increase by one. If the number of HAGBs in the complex with a given degree k is denoted by H_k, then the evolution of such numbers with random HAGBs generation will be given by [49]:

$$\frac{dH_k}{dp} = H_{k-1} - H_k \tag{10}$$

For each calculation step, when several faces become new HAGBs, the faces are increasing their degree by one, such that $H_{k-1} \to H_k$ and simultaneously $H_k \to H_{k+1}$ that change the number H_k. If H_k are normalised by the number of all GBs N_{GB} to obtain their fractions $h_k \le 1$, then with Laplace transformation Eq. (10) turns into the Poisson's distribution [49] for each degree:

$$h_k = \frac{p^k}{k!} e^{-p}. \tag{11}$$

Here the fraction of HAGBs p is analogue to discrete time. Numerical simulations naturally demonstrate the same Poisson behaviour for randomly generated HAGBs degrees in the discrete complex.

The set of TJs forms another quasi-random graph. The indices of TJs, i.e. the numbers of adjacent HAGBs, however, evolve in a rather different to GBs manner. These indices are limited by 3, and even for purely random generation of HAGBs their distributions can deviate significantly from the normal law. Hence, in our case, TJs evolve in a more complex manner even at pure random and homogeneous evolution of faces.

The evolutions of fractions of different types of triple junctions are shown in Fig. 9(a), (b). Dashed lines correspond to purely random generation of new HAGBs. Solid lines correspond to a second, "localized", mode, where the LAGBs converted to new HAGBs are those minimising the functional

$$N_{HAGB}^{o} \to \max(\alpha_1 N_{J0} + \alpha_2 N_{J1} + \alpha_3 N_{J2}), \tag{12}$$

where three coefficients $\alpha_i \sim 1$ define a propensity of each GB to be changed and N_{Ji} are the local numbers of TJs with type J_i bounding the selected GB. Numerical simulations revealed that the set $\{\alpha_1 = 1, \alpha_2 = 10, \alpha_3 = 5\}$ reflect well the experimental effect of micro-localization process in the studied Cu-Cr-Zr alloys. Evidently, the "localized" mode of HAGBs generation yields results in better agreement with the experimental points [26].

TJ fractions can be complemented with another, second-order, structural characteristic of TJs distribution, which measures the density

of HAGBs in the TJs vicinity, including and immediately beyond their adjacent HAGBs. If k is the index of a given TJ, i.e. the number of adjacent HAGBs, by summing up the index of the j-th TJ with the indices of its closest neighbours and normalising the result by their number, N_{neigh}^{j}, we define the degree of the j-th TJ by the expression:

$$TJ_i^{\deg} = \left(k + \sum_{neigh} k_{neigh}\right)/(1 + N_{neigh}^{j}) \tag{13}$$

The average TJ degree over all TJs, N_{TJ}, in the discrete complex is:

$$\langle TJ^{\deg}\rangle = \sum_j TJ_j^{\deg}/N_{TJ} \tag{14}$$

When all TJs are accounted for in the average, i.e. the junctions of type J_0 (TJs with adjacent LAGBs only) are included, the average degree provides an averaged state of GBs system of the complex, including the information about the inhomogeneity level of GBs spatial distribution. Results with included J_0 will be labelled with "All" in the next figures. When only HAGBs are accounted for in the average, i.e. the junctions of type J_0 are omitted, the average degree reflects only the inhomogeneity level of HAGBs distributions. Results with omitted J_0 will be labelled with "HAGB".

Fig. 10(a) shows the evolution of averaged through the discrete complex value of TJs HAGBs index $\langle TJ^{\deg}\rangle$ for the two cases. Both evolutions are plotted for pure random generation of new HAGBs (solid lines) as well as for "localized" mode of new HAGBs generation (dashed lines). The "All"-curves obtained with random and strongly localized generation of HAGBs are only slightly different. The "HAGB" curves on the other side show substantially different behaviour between the random and localized conversion approaches. The localized mode indicates a much more heterogeneous GB distribution. Exceeding the value of 3 (see the upper curve) shows the existence of some number of junctions with 4 "cube-like" and more adjacent grain boundaries. Dispersion of average degree (not shown on the figure) for both distributions of TJs is slightly different and is about 1.

Based on the "All" and "HAGBs" dependencies given by Eq. (14) and shown in Fig. 10(a) we propose an improved relation between grain and cell size for CDRX process written as:

$$d = \frac{D}{p}\nu. \tag{15}$$

This stems from Eqs. (4) and (9), where the homogeneity assumption is corrected by an effective frequency of TJs with HAGBs $\nu = \langle TJ_{All}^{\deg}\rangle/\langle TJ_{HAGBs}^{\deg}\rangle$, i.e. the ratio between the average degrees for "All" and for "HAGB". This frequency is a function of TJs spatial heterogeneity level expressed by TJs HAGBs degree.

Fig. 10(b) shows the grain size evolution predicted with and without accounting of just discussed inhomogeneities. The solid curve shows the calculation results by Eq. (4) with $J = p$. All experimental points are the same as have been presented in Fig. 8. The dashed line corresponds to the "localized" mode of GBs generation with grain size calculated by Eq. (16) according to dependences presented in Fig. 10(a). Obviously, possible heterogeneity in TJs spatial distribution leads to an additional decrease of grain size at high strains.

4.3. Further uses of the discrete approach

An interesting opportunity for the application of the discrete approach arises for predictions of ultrafine grains (UFGs) fraction. Suppose that the initial 3-cells represent dislocation cells, which can become UFGs, when most of the boundaries are converted to HAGBs during SPD simulation. Clearly, without full description involving grain boundary misorientations, many details cannot be captured, but an assumption that an initial dislocation cell becomes an UFG when more than half of its grain boundaries become HAGBs looks reasonable and corresponds to current microstructural observations. Fig. 11 shows the results from simulations based on this assumption together with experimental points from [26]. The very good correlation between simulations and experimental data lends strong support to the capabilities of the discrete approach.

One very important point in the comparison is that the simulations predict the appearance of the first UFG at the same accumulated strain of about 1 as observed experimentally. Another interesting point is the nonlinearity of both the experimental points and calculation curve. One can recognize the accumulated strain of 4 as a critical point, when the experimental curve should change its slope, reflecting HAGBs fraction behaviour shown in Fig. 7(b). The calculation curve also changes its behaviour at accumulated strain of 2, which corresponds to the dramatic changes in dislocation kinetics shown in Fig. 7(a). As a result, we can conclude that there are two critical points: about 2 and 4 accumulated strain, where the CDRX process in Cu-Zr alloys changes substantially. The first point corresponds to the formation of a large number of new HAGBs and.

a new system of grains, while the second one reflects the onset of a

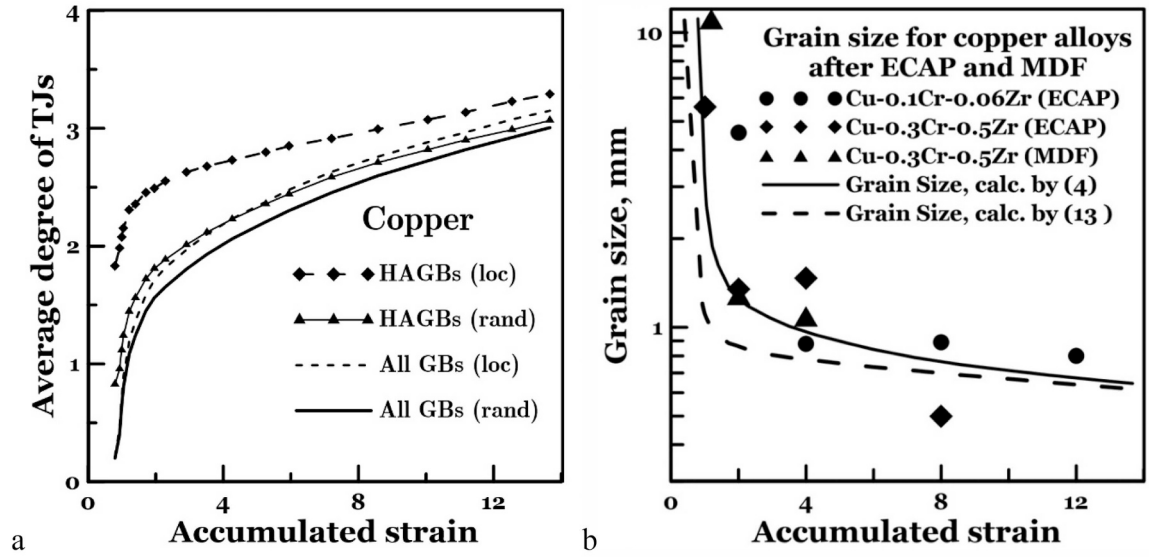

Fig. 10. (a): Evolution of TJs HAGBs degree. Label "All" corresponds to averaging over all TJs (including J_0 junctions); label "HAGBs" corresponds to averaging over TJs with indices larger than zero. Label "rand" corresponds to pure random generation of new HAGBs and "loc" means "localized" mode GBs evolution, according to Eq. (12). (b): Grain size evolution with and without account for TJs inhomogeneity.

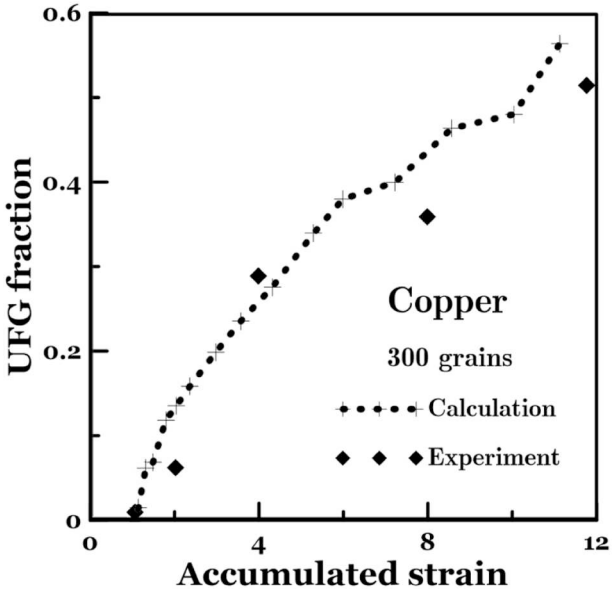

Fig. 11. Calculation of the UFG fraction by the discrete model comparing with experimental points [26].

new steady-state regime with partly stabilized grain structure. At the same time, the new system of grains continues to change slightly up to accumulated strain 12 and even more. HAGBs and UFG fractions at high values of accumulated strains keep increasing more intensely than other structural parameters, see Figs. 7(b) and 11.

5. Conclusions

The presented experimental and theoretical analysis of dynamic recrystallization in copper alloys reveals complex mechanisms controlling the evolution of defect structures in material undergoing severe plastic deformation, including micro-localization and macro-inhomogeneities of the plastic flow. These processes can be described by a set of material microstructural properties beyond the average grain size and microhardness of a sample typically measured in experimental works. Densities of dislocations for interiors and for boundaries of cells and grains, sizes of cells and grains, grain aspect ratio, fraction of the high-angle grain boundaries, volume fraction of triple junctions with a different number of adjacent high-angle grain boundaries, are among the parameters that can be measured experimentally and allow for improved theoretical predictions utilizing numerical simulations of SPD processes.

Separation of dislocations into mobile and immobile (or locked) dislocations and introduction of immobilization rate parameter [36] provides a possibility for "averaged" prediction of dislocation densities measured experimentally. Maximization of mobile dislocation density is observed for plastic strain ~1, for both the 1D and the 3D simulations. Additional dislocation drain described by Eq. (2), similarly to the one presented in [22], leads to maximization of the density of immobile dislocations for plastic strains ~2. For the studied alloys, fraction of high-angle grain boundaries demonstrates quasi-linear growth for plastic strains exceeding 2. Changes ongoing with dislocation cells and grain boundaries are generally similar (see Fig. 6), but differ dramatically in magnitude for small deformations, since the rate of size reduction for cells significantly exceeds the rate of refinement of grain structure. For large values of accumulated plastic strain (exceeding 8) the sizes of dislocation cells are differing from the grain sizes by several hundred nanometres and are not changing significantly for subsequent deformation. Two different SPD processes studied in this paper do not demonstrate substantial difference in the final microstructure of the processed materials. The dependency of fraction of HAGBs on accumulated strain for Cu-0.1Cr-0.06Zr alloy and Cu-0.3Cr-0.5Zr alloy almost coincide (see Fig. 5). At the same time, the sizes of grains and the sizes of dislocation cells for strains exceeding 2 are differing almost two times for the same materials (see Fig. 5).

Evolution of the high-angle grain boundaries in the process of severe plastic deformation, evolution of triple joints adjoining HAGBs and description of processes of micro- and macro-localization of plastic flow give a fairly realistic picture of physical processes in the bulk of severely deformed material. A wide range of microstructure parameters evaluated from a single specimen for two different copper alloys processed by two different SPD processes provided a possibility to test the applicability of the new model of dynamic recrystallization. The model accurately predicted the evolution of all of the material microstructure parameters based on the dependence of fraction of HAGBs on the plastic strain accumulated by material. The full three-dimensional modelling supplements the process by micro-localization taking place inside material grains (as observed in the experiment) and gives a possibility to reveal macroscopic inhomogeneities of plastic flow, demonstrating a much higher uniformity of deformation and microstructure of material after ECAP process in comparison to MDF. The combination of continuum finite element modelling with the newly proposed theoretical advances and discrete modelling of the microstructure offers a unique opportunity to study the effects of longer-scale structures on the emerging engineering scale behaviour of these and other alloys.

Acknowledgments

Morozova and Belyakov gratefully acknowledge the technical assistance of the Joint Research Center, "Technology and Materials", Belgorod State University. Borodin and Jivkov appreciate highly the financial support of EPSRC via grant EP/N026136/1 "Geometric Mechanics of Solids". Bratov declares no support from any scientific fund or program towards research presented here or preparation of this publication.

The authors confirm that the data supporting the findings of this study are available within the article.

References

[1] A. Vinogradov, Yu. Estrin, Analytical and numerical approaches to modelling of severe plastic deformation, Prog. Mater. Sci. 95 (2018) 172–242.
[2] K. Huang, R.E. Logé, A review of dynamic recrystallization phenomena in metallic materials, Mater. Des. 111 (2016) 548–574.
[3] T. Sakai, A. Belyakov, R. Kaibyshev, H. Miura, J.J. Jonas, Dynamic and post-dynamic recrystallization under hot, cold and severe plastic deformation conditions, Prog. Mater. Sci. 60 (2014) 130–207.
[4] Y. Estrin, A. Vinogradov, Extreme grain refinement by severe plastic deformation: a wealth of challenging science, Acta Mater. 61 (2013) 782–817.
[5] I. Sabirov, M.Yu. Murashkin, R.Z. Valiev, Nanostructured aluminium alloys produced by severe plastic deformation: new horizons in development, Mat. Sci. Eng. A 560 (2013) 1–24.
[6] C.C. Koch, T.G. Langdon, E.J. Lavernia, Bulk nanostructured materials, Metall and Mat Trans A 48 (2017) 5181–5199.
[7] M.J. Zehetbauer, Y.T. Zhu (Eds.), Bulk Nanostructured Materials, Willey-VCH, 2009.
[8] R.Z. Valiev, R.K. Islamgaliev, I.V. Alexandrov, Bulk nanostructured materials from severe plastic deformation, Prog. Mater. Sci. 45 (2000) 103–189.
[9] A.P. Zhilyaev, T.G. Langdon, Using high-pressure torsion for metal processing: fundamentals and applications, Prog. Mater. Sci. 53 (2008) 893–979.
[10] R.Z. Valiev, T.G. Langdon, Principles of equal-channel angular pressing as a processing tool for grain refinement, Prog. Mater. Sci. 51 (2006) 881–981.
[11] Y. Beygelzimer, R. Kulagin, Yu. Estrin, L.S. Toth, H.S. Kim, M.I. Latypov, Twist extrusion as a potent tool for obtaining advanced engineering materials: a review, Adv. Eng. Mater. 19 (8) (2017) 1600873(1–24p).
[12] J.G. Kim, M. Latypov, N. Pardis, Y.E. Beygelzimer, H.S. Kim, Finite element analysis of the plastic deformation in tandem process of simple shear extrusion and twist extrusion, Mater. Des. 83 (2015) 858–865.
[13] I.V. Khomskaya, V.I. Zel'dovich, E.V. Shorokhov, N.Yu. Frolova, I.N. Zhgilev, A.E. Kheifets, Structure formation in copper during dynamic channel-angular pressing, Phys. Metals Metallogr. 105 (2008) 586–593.
[14] V.I. Zel'dovich, S.V. Dobatkin, N. Yu, I.V. Frolova, A.E. Khomskaya, E.V. Kheifets, P.A. Shorokhov, Nasonov mechanical properties and the structure of chromium–zirconium bronze after dynamic channel-angular pressing and subsequent ageing, Phys. Met. Metallogr. 117 (1) (2016) 79–87.

[15] C. Xu, S. Schroeder, P.B. Berbon, T.G. Langdon, Principles of ECAP–conform as a continuous process for achieving grain refinement: application to an aluminum alloy, Acta Mater. 58 (2010) 1379–1386.
[16] M.J. Qarni, G. Sivaswamy, A. Rosochowski, S. Boczkal, Effect of incremental equal channel angular pressing (I-ECAP) on the microstructural characteristics and mechanical behaviour of commercially pure titanium, Mater. Des. 122 (2017) 385–402.
[17] C.N. Elias, M.A. Meyers, R.Z. Valiev, S.N. Monteiro, Ultrafine grained titanium for biomedical applications: an overview of performance, J. Mater. Research and Technology 2 (4) (2013) 340–350.
[18] A. Ma, C. Zhu, J. Chen, J. Jiang, D. Song, Shizhan Ni, Q. He, Grain refinement and high-performance of equal-channel angular pressed Cu-Mg alloy for electrical contact wire, Metals 4 (4) (2014) 586–596.
[19] S.C. Baik, Y. Estrin, H.S. Kim, R.J. Hellmig, Dislocation density-based modeling of deformation behavior of aluminium under equal channel angular pressing, Mater. Sci. Eng. A 351 (2003) 86–97.
[20] A. Mishra, B.K. Kad, F. Gregori, M.A. Meyers, Microstructural evolution in copper subjected to severe plastic deformation: experiments and analysis, Acta Mater. 55 (2007) 13–28.
[21] D.J. Lee, E.Y. Yoon, D. Ahn, B.H. Park, H.W. Park, L.J. Park, Y. Estrin, H.S. Kim, Dislocation density-based finite element analysis of large strain deformation behavior of copper under high-pressure torsion, Acta Mater. 76 (2014) 281–293.
[22] N.A. Enikeev, H.S. Kim, I.V. Alexandrov, Kinetic dislocation model of microstructure evolution during severe plastic deformation, Mater. Sci. Eng. A 460–461 (2007) 619–623.
[23] I.V. Alexandrov, R.G. Chembarisova, V.D. Sitdikov, Analysis of the deformation mechanisms in bulk ultrafine grained metallic materials, Mat. Sci. Eng. A 463 (2007) 27–35.
[24] A.A. Smolyakov, V.P. Solovyev, A.I. Korshunov, N.A. Enikeev, Three-dimensional numerical simulations of multi-pass equal-channel angular pressing by a variation difference method and comparison with experiment, Mat. Sci. Eng. A 493 (2008) 148–159.
[25] A. Belyakov, T. Sakai, H. Miura, K. Tsuzaki, Grain refinement in copper under large strain deformation, Phil. Mag. A 81 (2001) 2629–2643.
[26] A. Morozova, E. Borodin, V. Bratov, S. Zherebtsov, A. Belyakov, R. Kaibyshev Grain refinement kinetics in a low alloyed Cu–Cr–Zr alloy subjected to large strain deformation, Materials 10 (2017) 1394.
[27] W. Skrotzki, A. Pukenas, B. Joni, E. Odor, T. Ungar, A. Hohenwarter, R. Pippan, E.P. George, Microstructure and texture evolution during severe plastic deformation of CrMnFeCoNi high-entropy alloy, IOP Conf. Series: Mat. Sci. Eng. 194 (2017) 012028.
[28] E.N. Borodin, V. Bratov, Non-equilibrium approach to prediction of microstructure evolution for metals undergoing severe plastic deformation, Mater. Charact. 141 (2018) 267–278.
[29] I. Shakhova, Z. Yanushkevich, I. Fedorova, A. Belyakov, R. Kaibyshev, Grain refinement in a Cu–Cr–Zr alloy during multidirectional forging, Mat. Sci. Eng. A 606 (2014) 380–389.
[30] G. Purcek, H. Yanar, M. Demirtas, Y. Alemdag, D.V. Shangina, S.V. Dobatkin, Optimization of strength, ductility and electrical conductivity of Cu–Cr–Zr alloy by combining multi-route ECAP and aging, Mat. Sci. Eng. A 649 (2016) 114–122.
[31] K. Abib, H. Azzeddine, K. Tirsatine, T. Baudin, A.-L. Helbert, F. Brisset, B. Alili, D. Bradai, Thermal stability of cu-Cr-Zr alloy processed by equal-channel angular pressing, Mater. Charact. 118 (2016) 527–534.
[32] K. Valdés León, M.A. Munoz-Morris, D.G. Morris, Optimisation of strength and ductility of cu–Cr–Zr by combining severe plastic deformation and precipitation, Mat. Sci. Eng. A 536 (2012) 181–189.
[33] A.P. Zhilyaev, I. Shakhova, A. Morozova, A. Belyakov, R. Kaibyshev, Grain refinement kinetics and strengthening mechanisms in Cu–0.3 Cr–0.5 Zr alloy subjected to intense plastic deformation, Mat. Sci. Eng. A 654 (2016) 131–142.
[34] A. Morozova, R. Kaibyshev, Grain refinement and strengthening of a Cu–0.1 Cr–0.06 Zr alloy subjected to equal channel angular pressing, Phil. Mag. 97 (24) (2017) 2053–2076.
[35] M.A. Meyers, K. Chawla, Mechanical Behavior of Materials, Cambridge University Press, 2009.
[36] A.E. Mayer, K.V. Khishchenko, P.R. Levashov, P.N. Mayer, Modeling of plasticity and fracture of metals at shock loading, Appl. Phys. J. 113 (2013) 193508.
[37] R. Lapovok, F.H. Dalla Torre, J. Sandlin, C.H.J. Davies, E.V. Pereloma, P.F. Thomson, Y. Estrin, Gradient plasticity constitutive model reflecting the ultrafine micro-structure scale: the case of severely deformed copper, J. Mech. Phys. Solids 53 (2005) 729–747.
[38] G.A. Malygin, Dislocation self-organization processes and crystal plasticity, Physics-Uspekhi 169 (1999) 979.
[39] A.E. Dudorov, A.E. Mayer, Equations of dislocation dynamics and kinetics at high rates of plastic deformation, Vestn. Chelyabinsk State Univ. Phys. 39 (2011) 12.
[40] E.I. Galindo-Nava, P.E.J. Rivera-Dıaz-del-Castillo, A thermodynamic theory for dislocation cell formation and misorientation in metals, Acta Mater. 60 (2012) 4370–4378.
[41] E.I. Galindo-Nava, P.E.J. Rivera-Diaz-del-Castillo, A thermo-statistical theory of low and high temperature deformation in metals, Mater. Sci. Eng. A 543 (2012) 110–116.
[42] E.I. Galindo-Nava, J. Sietsma, P.E.J. Rivera-Diaz-del-Castillo, Dislocation annihilation in plastic deformation: II. Kocks-Mecking analysis, Acta Mater. 60 (2012) 2615–2624.
[43] A. Vinogradov, Mechanical properties of ultrafine-grained metals: new challenges and perspectives, Adv. Eng. Mater. 17 (12) (2015) 1710–1722.
[44] M.A. Meyers, V.F. Nesterenko, J.C. La Salvia, Y.B. Xu, Q. Xue, Observation and modeling of dynamic recrystallization in high-strain, high-strain rate deformation of metals, J. Phys. IV France 10 (2000) 51–56.
[45] M. Frary, C.A. Schuh, Percolation and statistical properties of low- and high-angle interface networks in polycrystalline ensembles, Phys. Rev. B 69 (2004) 134115.
[46] L.J. Grady, J.R. Polimeni, Discrete Calculus, Springer-Verlag, London, 2010.
[47] Voro++ free software, available at http://math.lbl.gov/voro++.
[48] VoroC++Analyzer (VCA) is available for free at, https://mapos.manchester.ac.uk.
[49] P.L. Krapivsky, S. Redner, E. Ben-Naim, A Kinetic View of Statistical Physics, Cambridge University Press, 2010.